Supporting Information for

Excitation polarization modulation in localization microscopy allows to resolve structure of individual non-blinking nano-objects

D. Thomsson†, G. Sforazzini‡, H. L. Anderson‡ and I. G. Scheblykin†*

† *Chemical Physics, Lund University, Box 124, 22100, Lund, Sweden*
*Email: ivan.scheblykin@chemphys.lu.se*
‡ *Chemistry Research Laboratory, Department of Chemistry, University of Oxford, Mansfield Road, Oxford, OX1 3TA (UK)*

1. Sample preparation

The polymer

For the sample preparation the polystyrene (PS) was dissolved in toluene (10 mg/mL). PFBV-Rtx (Fig. S-1) was also dissolved in toluene at low concentrations and mixed with the PS/toluene solution. The weight-to-weight ratio of PFBV-Rtx/PS was 10^{-7}. PFBV-Rtx/PS solutions were spin cast on cleaned quartz substrates resulting in ~ 200 nm thick PS films. DXP was also immobilized in PS films using the same technique.

Figure S-1. Chemical structure of the polymer
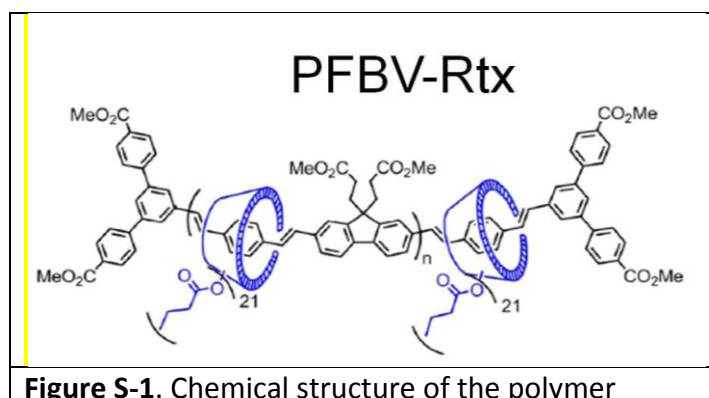
DXP dye

To calibrate the setup we used *N,N'*-bis(2,6-dimethylphenyl)perylene-3,4,9,10-tetracarboxylic diimide (DXP). This dye is commercially available from Aldrich. DXP molecules were dissolved in toluene. Mixing with a PS/toluene solution followed by spin casting on cleaned quarts substrates resulted in 200 nm thick DXP/PS films with w/w ratio of ~ 10^{-3} to 10^{-4}.

2. Centroid function localization

Two-dimensional (2D) Gaussian functions

$$f(x, y) = A \exp\left(-\frac{(x-x_0)^2}{2\sigma_x^2} - \frac{(y-y_0)^2}{2\sigma_y^2} \right)$$

(S-1)

were fitted to the fluorescence centroid using a weighted nonlinear least square fit:

$$\chi^2 = \frac{1}{2}\sum_{k=1}^{N}\frac{(u_i - f_i)^2}{\sigma_i^2} \qquad \text{(S-2)}$$

The weight factor σ_i in eq. S-2 is a sum of the variances of the photon counting noise and the variance of the background.[1] So $\sigma_i^2 = \sigma^2{}_{\text{photon }i} + \sigma_{\text{BG}}{}^2$ or $\sigma_i^2 = f_i + \sigma_{\text{BG}}{}^2$ since the expectation value is equal to the variance for the Poisson distribution. A nonlinear Levenberg-Marquardt algorithm was used to find the best fit.

3. Chung-Kennedy (C-K) algorithm

The measured time-dependence of the centroid positions (x, y) of the 2D Gaussian functions were filtered with an edge preserving filter (Chung-Kennedy (C-K) algorithm)[2-5] in order to decrease the localization error. The C-K filter is a nonlinear filter that statistically evaluates data in a window of length (w) before and after the sampled data point i. The idea is to calculate predictors based on the events before and after i. The predictors are then used to weight so-called estimators, which are calculated for the same historical and future events. The notations below follow those in reference.[5] The first step is to calculate the mean values (estimators) for the windows in front of (+) and behind (-) the data point i.

$$X_{i\pm} = \frac{1}{w}\sum_{k=1}^{w}x_{i\pm k} \qquad \text{(S-3)}$$

The length of the window can be chosen arbitrarily. For the same windows as in equation (3) the variances are calculated:

$$\sigma_{i\pm}^2 = \frac{1}{w}\sum_{k=1}^{w}\left(x_{i\pm k} - X_{i\pm}\right)^2 \qquad \text{(S-4)}$$

The variances are used to calculate the predictors[4] or, in other words, switching factors g:[5]

$$g_{i+} = \frac{\left(\sigma_{i-}^2\right)^p}{\left(\sigma_{i+}^2\right)^p + \left(\sigma_{i-}^2\right)^p} \qquad \text{(S-5)}$$

$$g_{i-} = \frac{\left(\sigma_{i+}^2\right)^p}{\left(\sigma_{i-}^2\right)^p + \left(\sigma_{i+}^2\right)^p} \qquad \text{(S-6)}$$

The nonlinear parameter p can be chosen arbitrarily. A useful range is [1, 100].[4] Using $p = 0$ converts the nonlinear filter into a regular linear filter i.e. a nearest neighbor smoothing filter. The number of data points that are included in the smoothing is determined by the size of the window. The denominators are used for the normalization:

$$g_{i-} + g_{i+} = 1 \qquad \text{(S-7)}$$

The filtered output is given by

$$X_{out}(i) = g_{i+}X_{i+} + g_{i-}X_{i-} \qquad \text{(S-8)}$$

In the end the optimal choice of the parameters p and w is determined by the experimental data including the features of the noise. We used $p = 1$ and $w = 10$ for our experiments. The nonlinearity was still high enough to consider the filter to be significantly different from the linear filter.

4. Error Estimation
Several factors contribute to the errors in the localization accuracy. First of all there are fundamental reasons like photon counting noise, pixelation noise and background emission.

The detector (CCD camera) introduces an additional dark noise and a readout noise. Secondly there are errors which originate from the mechanical parts of the experimental setup. These could be due to changes in the pressure of the gas flow (if a gas chamber with a continuous flow is used) or mechanical vibrations or stress in the optical elements. Moving parts can introduce a systematic drift which is identical for all imaged objects in the experiment.

An expression for the fundamental errors without the drift was derived by Thompson et.al.[1]. In their paper a discrepancy of 30 % between their analytical and numerical calculations was reported which has been recently explained by Mortensen et.al. [6]

$$\varepsilon^2 = \frac{\sigma^2}{N} + \frac{p^2}{12N} + \frac{8\pi\sigma^4 b^2}{p^2 N^2} \qquad \text{(S-9)}$$

Here σ is the standard deviation of the centroid, p is the effective pixel size and b is the standard deviation of the background intensity (in number of photons).

In our work the numerical simulations and the control experiments on single dyes constituted the basis for the error estimations. Numerically and experimentally obtained values were compared with the expected errors (according to equation (9)) for the particular experimental settings.

5. Image drift

The image drift is different in each experiment and must be compensated for. One way to do that is by using a reference object like a fluorescent bead[3] which moves together with the sample. Another way is to do the compensation by using the information from several objects which experienced the same drift and to calculate their average positions. The latter procedure was the one chosen in this work. Examples of the localization drift are shown in figure S-2. By choosing carefully a set of molecules for the average calculation the drift can be compensated for with a reasonable accuracy. Only the most stable molecules were chosen for this purpose. Once the average positions i.e. the drift were calculated the positions for all molecules in the same experiment could be corrected. If the correction is not successful all molecules will show a systematic error in the x, y position plots. Typically the data are elongated in some direction which is the same for all molecules in the given experiment.
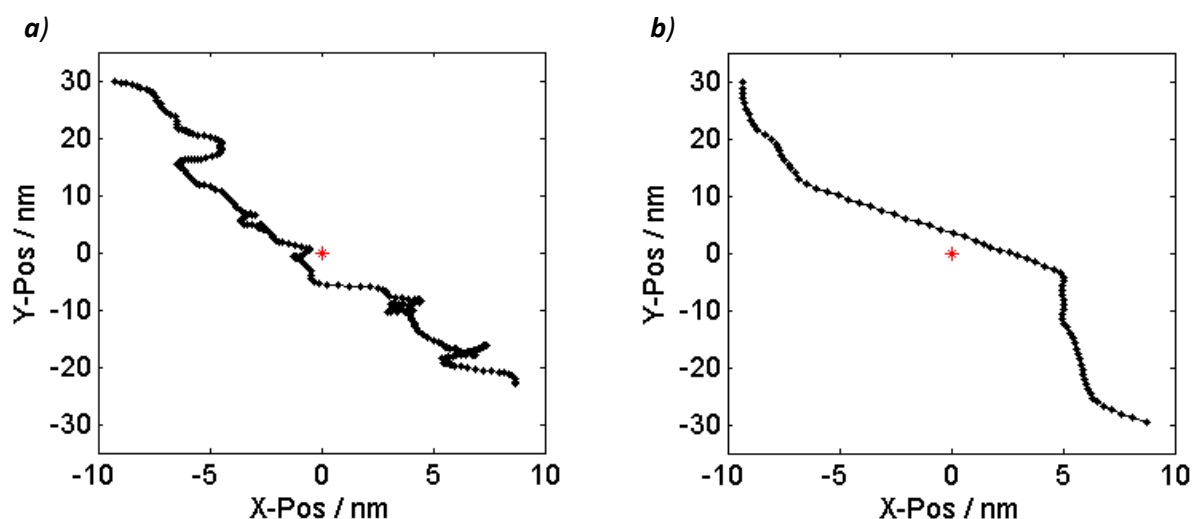

Figure S-2. Examples of the image drift. (**a**) Six single PFBV-Rtx chains were used to calculate the average positions for the drift compensation. (**b**) Drift in the localization data for a sample with DXP dyes. Five dye molecules were used to construct the average drift. The drift could successfully be compensated for in both cases. The image exposure time in these two experiments was different: polymer - t_{exp} = 0.5 s, dyes - t_{exp} = 2.5 s.

6. Experimental errors and check of the drift compensation

In order to test the entire data handling from the acquiring to plotting and to get an estimation of the errors where all sources were included we carried out experiments on DXP molecules. In order to have a comparable signal to noise for single dyes and single polymer chains an excitation density of 260 W·cm^{-2} together with an exposure time of ~ 2.5 s was used. These numbers can be compared with those for the PFBV-Rtx polymer where the excitation density and exposure time was ~ 60 W·cm^{-2} and 0.5 s respectively.

The DXP sample was irradiated for about 20 minutes in order to bleach most of the molecules. Only few (the most stable ones) molecules remained strongly emissive after the irradiation treatment and were stable during the experimental time ~ 250 s. The effective concentration of the "useful" emissive molecules was comparable to that for a typical polymer sample used (see figure S-3).

t = 0 min t = 20 min t = 20 min
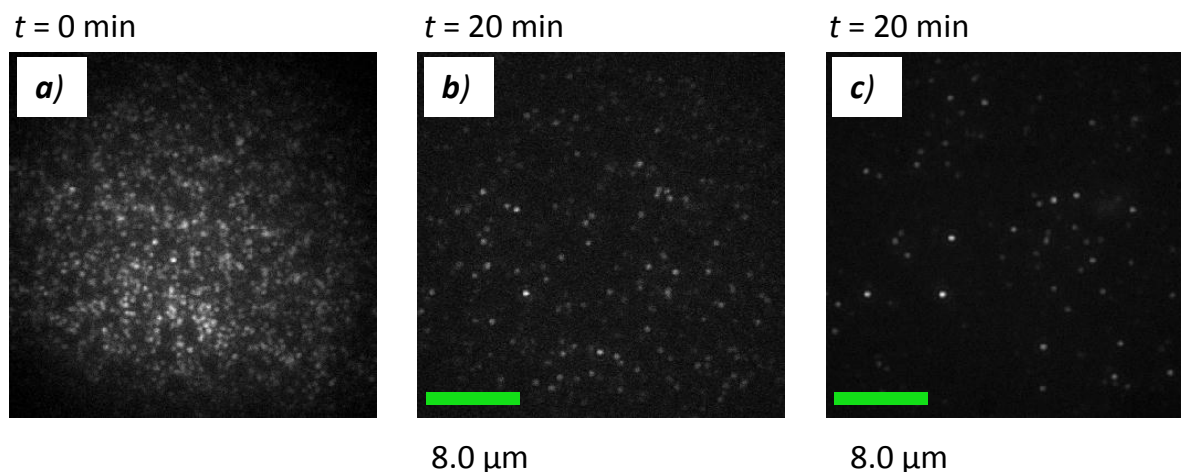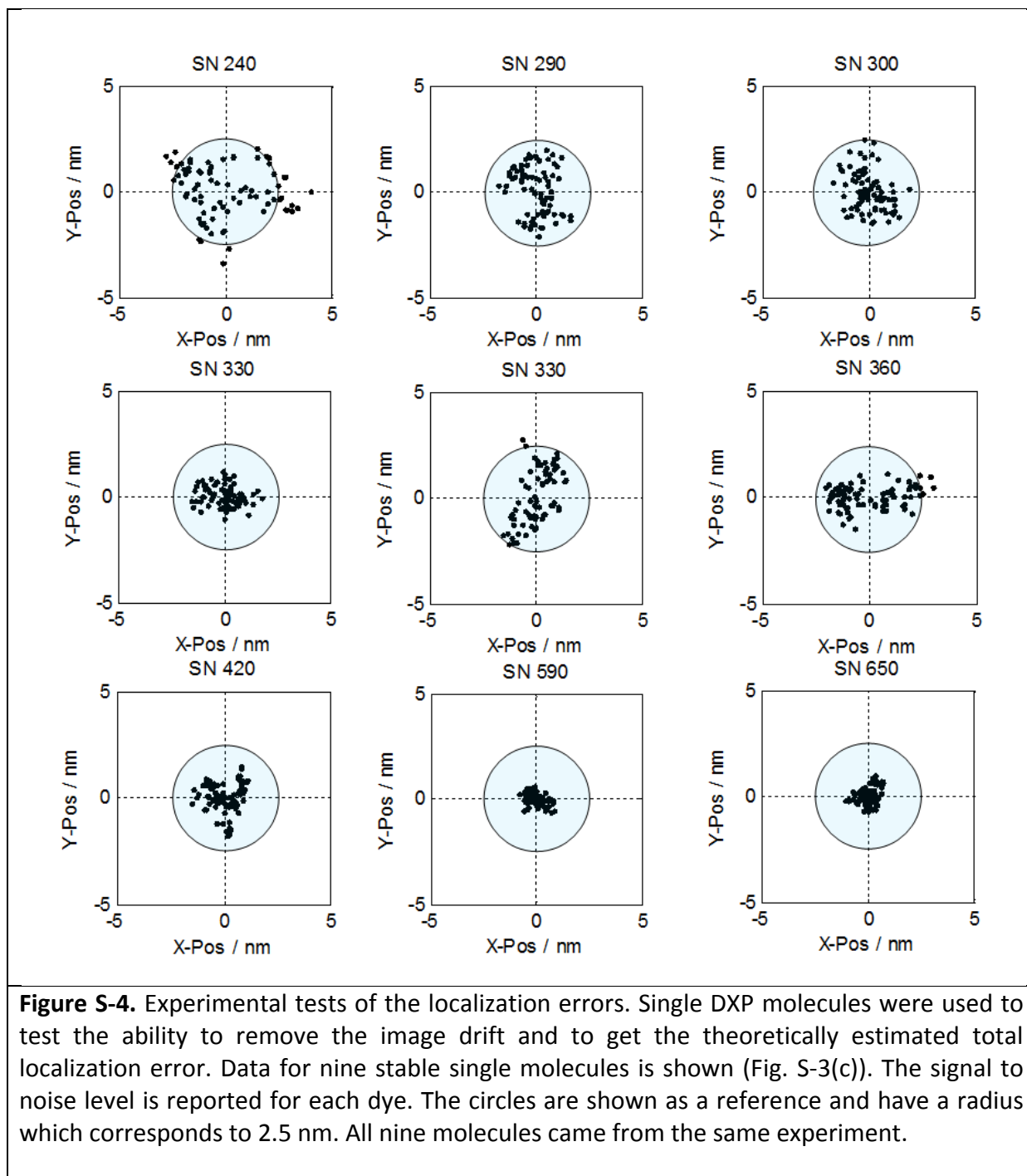

8.0 µm   8.0 µm

Figure S-3. Test of error estimations by localization experiments on DXP dyes. (*a*) Dyes were mixed with PMMA at a relatively high concentration. The exposure time for the image (*a*) was 0.2 s. (*b*) After 20 minutes of laser irradiation with an excitation density of 260 Wcm^{-2} only few stable dyes remained (exposure time 0.2 s). (*c*) A second DXP/PMMA sample after 20 minutes of irradiation. The exposure time was 2.5 s for the image (*c*). Localization data for nine molecules obtained from the sample in (*c*) is shown in Figure S-4.
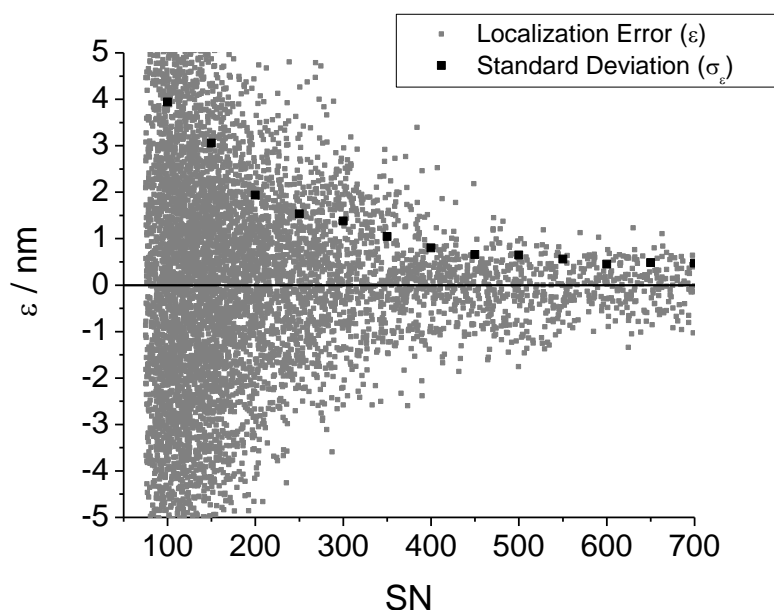
Figure S-4 shows the localization data for nine single molecules from Figure S-3(c). Together with the localization data circles are drawn. The radius of each circle is 2.5 nm giving the scale to the picture. For each molecule the average signal to noise ratio (SN) is reported. The spread in localization can be compared to the expected errors shown in figure S-5.

4

Figure S-4. Experimental tests of the localization errors. Single DXP molecules were used to test the ability to remove the image drift and to get the theoretically estimated total localization error. Data for nine stable single molecules is shown (Fig. S-3(c)). The signal to noise level is reported for each dye. The circles are shown as a reference and have a radius which corresponds to 2.5 nm. All nine molecules came from the same experiment.

In order to test further the data analysis addition simulations were carried out. Two-dimensional Gaussian functions (eq. S-3) were generated. Different levels of normally distributed noise (N) were added to the generated functions. The signal to noise was characterized by the signal amplitude B, which was kept constant, and the gradually increasing noise N.

$$f(x, y) = B \exp\left(-\frac{(x-x_0)^2}{2\sigma_x^2} - \frac{(y-y_0)^2}{2\sigma_y^2}\right) + N \qquad \text{(S-10)}$$

In figure S-5 the localization error is plotted against signal to noise. The standard deviation of the localization error was calculated for different SN intervals as well. The first interval was calculated as $\Delta SN_1 = SN_{HIGH,\ 1} - SN_{LOW,\ 1} = 125 - 75 = 50$. The procedure was repeated for twelve equally sized intervals. The calculated standard deviations are shown as black squares in figure S-5.

The standard deviations σ_ε in figure S-5 and the experimental data in figure S-4 show only moderate differences. It is therefore possible to conclude that the drift (shown in figure S-2(b)) does not contribute significantly to the localization error once it has been accounted for.

Figure S-5. The localization error (ε) as a function of signal to noise (SN). Gray squares; localization errors obtained from simulations. Black squares; standard deviations (σ_ε) of the localization error calculated in intervals of $\Delta SN = 50$, starting at SN = 75.

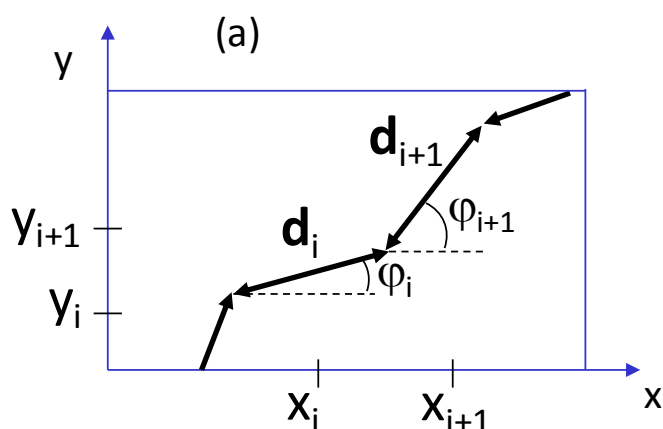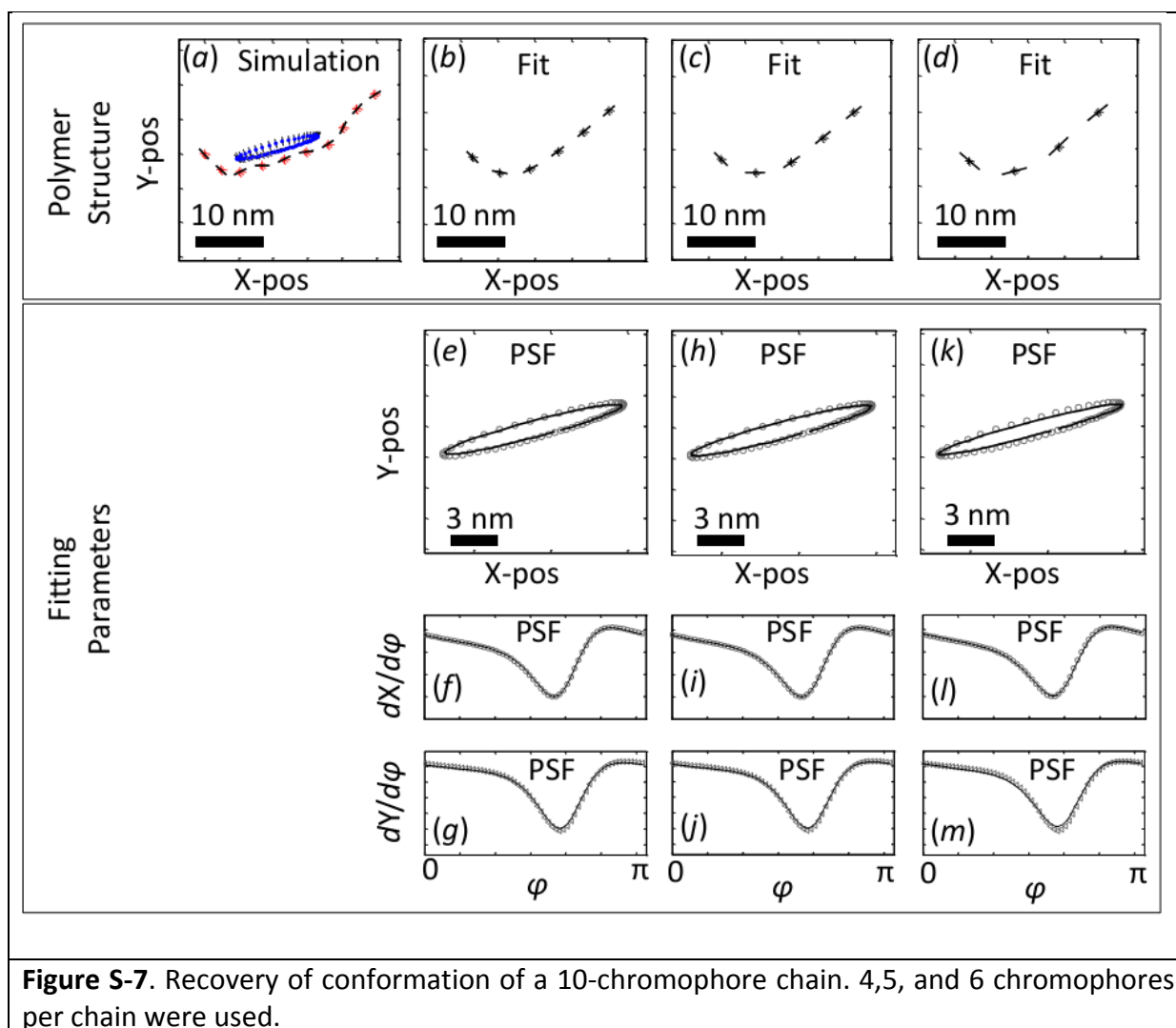## 7. Notes on the chain conformation recovery

Figure S-6. Parameters of a multi-chromophore chain

When N chromophores of the same length are connected to each other (Fig. S-6) the number of parameters fully determining the chain geometry is reduced from $3N$ (for each chromophore we need to know two coordinates and one angle) to coordinates of the first chromophore and N angles ($N+2$).

6

Notes to Fig. S-7 and Fig. 3. We want to stress that the fits for $N = 6$ are better than those for $N = 4$ even though it is not easily seen in the Fig. S-7. It should also be mentioned that a poor match between the original and the regenerated chain never coincides with a good fit of the centroid position and the coordinate derivatives.

In connection to Fig. S-7 we would also like to mention that a successful fit of $N = 6$ or 5 dipoles to a system consisting of ten is quite unusual with the presented method. A possible improvement which has not been tried yet is to start with even lower number of dipoles initially e.g. $N = 2$ or 3. Fitted parameters for the model with $N = 3$ could then be used to calculate the starting parameters for the system with $N = 4$. This procedure could be repeated few times increasing the chance for the successful fit.

Figure S-7. Recovery of conformation of a 10-chromophore chain. 4,5, and 6 chromophores per chain were used.

8. Influence of the emission polarization on the localization accuracy

In general the fluorescence intensity centroid of an infinitely small object (point spread function (PSF)) is not completely symmetric unless the polarization anisotropy[7,8] of the object is close to zero. If the transition dipole moment of a single dye molecule (emission is fully polarized) is oriented in the sample plane the PSF is not rotationally symmetric relative to the optical axis, however, the middle point still coincides with the object location. However, if the transition dipole moment is oriented out of the plane with an angle $< 90°$ the intensity

maximum of the PSF will be shifted relative to the actual physical position of the object. This type of asymmetry affects the localization accuracy [9], the larger the objective lens NA the larger the effect. According to the calculations[9] if NA<1.1 for the extreme case of a single dipole in the sample plane the maximum localization error is smaller than 2.5 nm. However, since in our case the fluorescence of PFBV-Rtx chains is only partially polarized with an average polarization degree of 0.5 [10] the localization error must be significantly smaller. Therefore, the localization error due to the fluorescence light polarization can be neglected in comparison with the centroid shifts correlated with the excitation light polarization (Fig. 5 of the main article).

The asymmetry of the centroid shape can be measured by the ratio of the widths σ_x/σ_y of the fitted Gaussian functions. In figure S-8 the ratios σ_x/σ_y are shown for the four molecules.
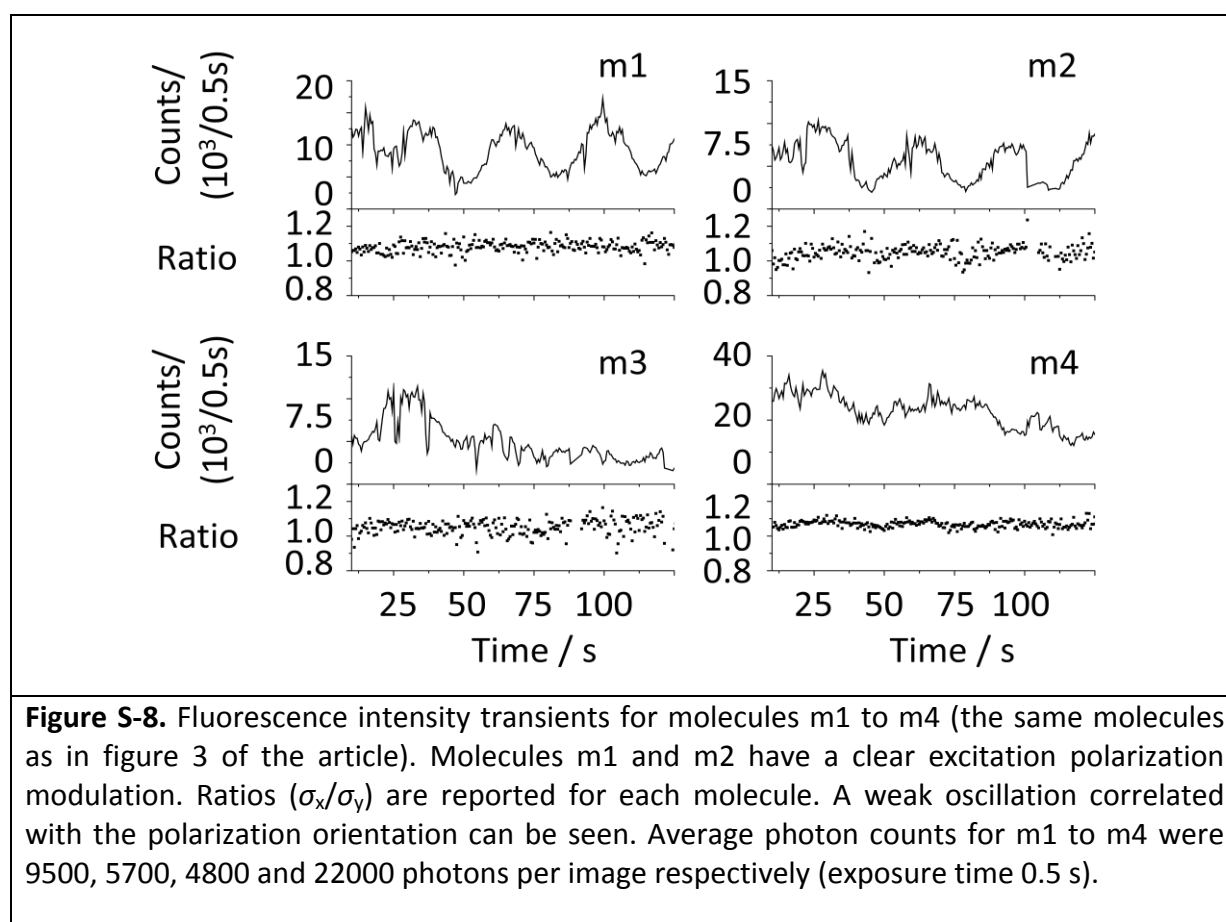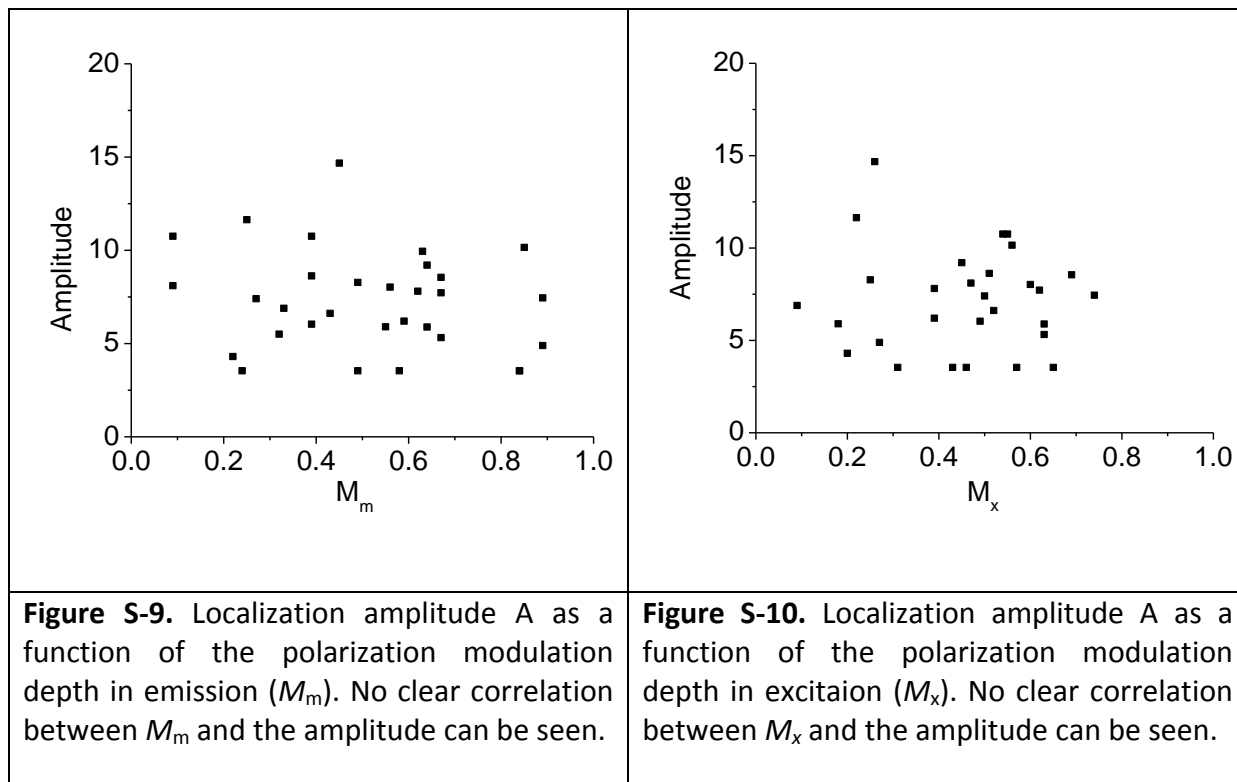

Figure S-8. Fluorescence intensity transients for molecules m1 to m4 (the same molecules as in figure 3 of the article). Molecules m1 and m2 have a clear excitation polarization modulation. Ratios (σ_x/σ_y) are reported for each molecule. A weak oscillation correlated with the polarization orientation can be seen. Average photon counts for m1 to m4 were 9500, 5700, 4800 and 22000 photons per image respectively (exposure time 0.5 s).

Some oscillations in σ_x/σ_y can be indeed seen for m2, m3 and m4. We believe that this is because for an anisotropic system without complete energy transfer the fluorescence polarization degree is dependent on the excitation polarization angle.[8,11] Basically the photoselection determines which subset of the chromophores within the single chain that emits the most. Upon rotation of the excitation polarization the subset of chromophores changes leading to fluorescence polarization change and, as a consequence, a change of the PSF asymmetry ratio σ_x/σ_y.

The effect of light polarization on the centroid localization, if significant, should be correlated with the polarization anisotropy of the molecules. Therefore for PFBV-Rtx we plot the average polarization degree (or modulation depth[8]) in excitation, M_x, or in emission, M_m, against the average localization amplitude A defined by eq. S-2 in the main text. Data for 37 molecules are shown in figure S-9 and S-10. No correlation could be seen. Polarization

parameters were measured before the super-resolution imaging was carried out therefore only molecules with minor photobleaching were included.

Figure S-9. Localization amplitude A as a function of the polarization modulation depth in emission (M_m). No clear correlation between M_m and the amplitude can be seen.

Figure S-10. Localization amplitude A as a function of the polarization modulation depth in excitaion (M_x). No clear correlation between M_x and the amplitude can be seen.
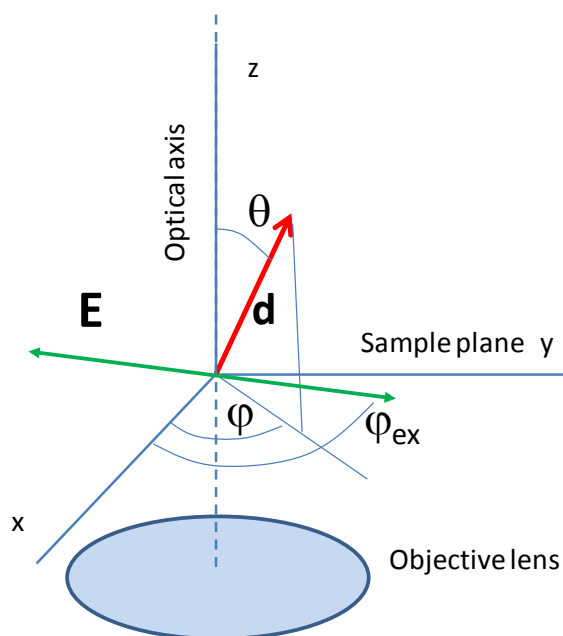
9. Fluorescence brightness of a single molecule

Figure S-11

d – vector of the transition dipole moment

E – vector of the excitation light electric field

Fluorescence is collected by the same objective lens.

According section 3.2 of the paper, in the case of low *NA* in excitation, intensity of the fluorescence collected by the objective lens with numerical aperture NA_c is:

$$I_{fl.coll} = I_{ex} \cdot \sigma \cdot \Phi \cdot A(\theta, NA_c) \cdot \sin^2\theta \cdot \cos^2(\varphi - \varphi_e) = 2I_{ex}B(\theta, NA_c) \cdot \cos^2(\varphi - \varphi_e)$$
$$B(\theta, NA_c) = \tfrac{1}{2}\sigma \cdot \Phi \cdot A(\theta, NA_c)$$

(S-11)

where A is the fluorescence collection efficiency, Φ is fluorescence quantum yield of the chromophore, I_{ex} – excitation power density, σ - absorption cross section of the chromophore at the excitation wavelength, B – fluorescence brightness.{Lin, 2010 581 /id}

Since the emission of the chromophore can be represented as the sum of the emissions of two chromophores with the absorption cross sections $\sigma\cos^2\theta$ and $\sigma\sin^2\theta$ oriented along Z-axis and within the XY plane respectively we can re-write the collection efficiency A as follows:

$$A(\theta, NA_c) = A_{Z\,component} + A_{XY\,component} = a(NA_c) \cdot \left(A_z(\theta, NA_c)\cos^2\theta + \sin^2\theta\right)$$

(S-12)

where a does not depend on the orientation of the dipole.

Then the Eq.4 can be re-rewritten as follows:

$$I_{fl.coll} = I_{ex} \cdot \sigma \cdot \Phi \cdot a(NA_c) \cdot \left(A_z(\theta, NA_c)\cos^2\theta + \sin^2\theta\right)\sin^2\theta \cdot \cos^2(\varphi - \varphi_e)$$

(S-13)

And fluorescence brightness then is

$$B(\theta, NA_c) = \tfrac{1}{2} \cdot \sigma \cdot \Phi \cdot a(NA_c)\left(A_z(\theta, NA_c)\cos^2\theta + \sin^2\theta\right)\sin^2\theta$$

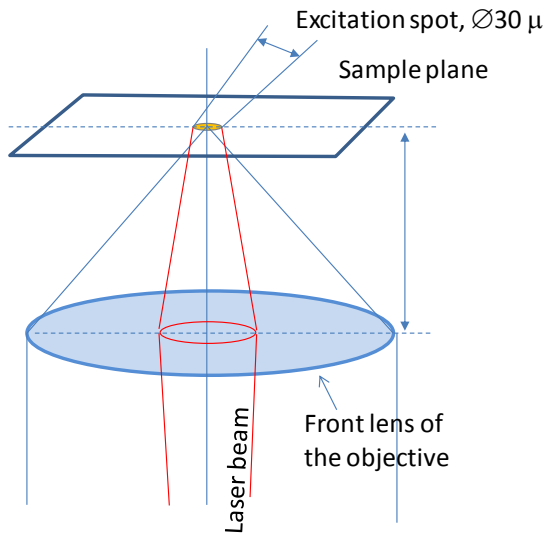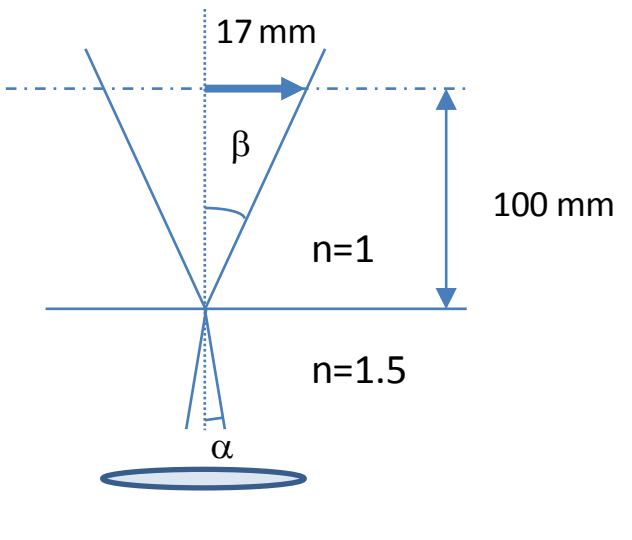The dependence of brightness on θ retains even for small NA_c.
If $NA_c \to 0$, then $A_z = 0$, and the overall θ-dependence of the fluorescence intensity is $\sin^4\theta$:

$$B(\theta) = \tfrac{1}{2}a(NA_c)\sin^4\theta$$
$$I_{fl.coll} = I_{ex} \cdot a(NA_c) \cdot \sin^4\theta \cdot \cos^2(\varphi - \varphi_e)$$
$$if \quad NA_c \to 0$$

(S-14)

10. Estimation of NA in excitation

Figure S-12	**Figure S-13**
Sample excitation scheme	To the calculation of the NA in excitation. $\beta = 9.6^{\circ}$; $1.5 * \sin \alpha = \sin \beta$; $\alpha = 6.4^{\circ}$ $NA_{ex} = n \sin \alpha = 0.17$

Before reaching the objective lens, the excitation laser beam was de-collimated by a lens with 300 mm focal distance. That is why the laser is focused slightly above the sample plane creating excitation spot of 20μ in diameter (see fig. S-12). The diameter of the laser beam at the back lens of the objective lens was ca 0.7 mm, while the diameter of the back lens of the objective was 7 mm. That is why the NA in excitation was much less than the maximum achievable with the current objective lens (1.25).

We estimated the maximum inclination angle of the laser light to the optical axis at the sample plane (α) by measuring the laser beam radius at a certain distance from the objective lens (Fig. S-13). The results of the measurements and calculations are given in the Fig.S-13 caption.

Inclination angle of 6.4 degrees is very small, $NA_{ex} = 0.17$. So, the excitation was done in the regime close to the paraxial limit.

[1] R.E. Thompson, D.R. Larson, and W.W. Webb, *Biophysical Journal*, 2002, **82**, 2775-2783.
[2] S. Habuchi, S. Onda, and M. Vacha, *Physical Chemistry Chemical Physics*, 2011, **13**, 1743-1753.
[3] S. Habuchi, S. Onda, and M. Vacha, *Chemical Communications*, 2009, 4868-4870.
[4] S.H. Chung and R.A. Kennedy, *Journal of Neuroscience Methods*, 1991, **40**, 71-86.

[5] D.A. Smith, *Philosophical Transactions of the Royal Society of London Series B-Biological Sciences*, 1998, **353**, 1969-1981.

[6] K.I. Mortensen, L.S. Churchman, J.A. Spudich, and H. Flyvbjerg, *Nature Methods*, 2010, **7**, 377-U59.

[7] D.H. Hu, J. Yu, K. Wong, B. Bagchi, P.J. Rossky, and P.F. Barbara, *Nature*, 2000, **405**, 1030-1033.

[8] O. Mirzov, R. Bloem, P.R. Hania, D. Thomsson, H.Z. Lin, and I.G. Scheblykin, *Small*, 2009, **5**, 1877-1888.

[9] J. Enderlein, E. Toprak, and P.R. Selvin, *Opt. Express*, 2006, **14**, 8111-8120.

[10] R. Camacho, D. Thomsson, G. Sforazzini, H.L. Anderson, and I.G. Scheblykin. Inhomogeneous quenching as a limit of the correlation between fluorescence polarization and conformation of single molecules. 2013. Submitted to JPC Letters

[11] R. Camacho, D. Thomsson, D. Yadav, and I.G. Scheblykin, *Chem. Phys.*, 2012, **406**, 30-40.